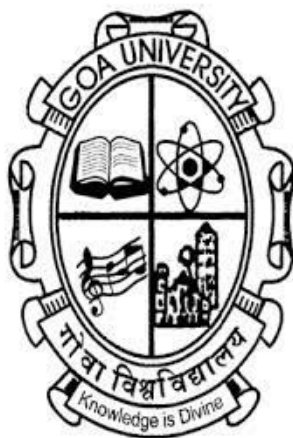


COBALT CATALYSTS
FOR
ELECTROCHEMICAL REDUCTION
OF
CARBON DIOXIDE

A M.Sc. DISSERTATION REPORT BY:

DAPHNE D'SILVA



SCHOOL OF CHEMICAL SCIENCES

GOA UNIVERSITY

GOA 403206

APRIL 2022

LITERATURE SURVEY ON
COBALT CATALYSTS
FOR
ELECTROCHEMICAL REDUCTION
OF
CARBON DIOXIDE

A DISSERTATION REPORT

Submitted In Partial Fulfilment of The Degree

Of

M.Sc. (Physical Chemistry)

By

Miss Daphne D'silva

To The

School Of Chemical Sciences

Goa University

Goa 403206

April 2022

CERTIFICATE

This is to certify that the dissertation entitled “**Literature Survey on Cobalt Catalysts for Electrochemical Reduction of Carbon Dioxide**” is bonafide work carried out by Miss Daphne D’silva under my supervision in partial fulfilment of the requirement for the award for the award of the degree of Master of Science in Chemistry at the School of Chemical Sciences, Goa University.

Dr. Pranay Morajkar
Guiding Teacher
School of Chemical Sciences
Goa University

Prof. Dr. Vidhyadatta Verenkar
Dean
School of Chemical Sciences
Goa University

STATEMENT

I hereby declare that the matter presented in this dissertation entitled “**Literature Survey on Cobalt Catalysts for Electrochemical Reduction of Carbon Dioxide**” is based on results of investigation carried out by me in School of Chemical Science, Goa University under the supervision of Dr. Pranay Morajkar and the same has not been submitted elsewhere for the award of the degree or diploma.

Daphne D'silva

20P0490020

TABLE OF CONTENTS

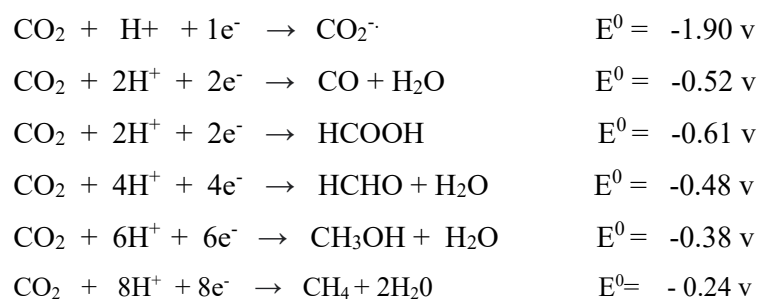
I.	INTRODUCTION	7
II.	SYNTHESIS, CHARACTERISATION AND ELECTROLYSIS	10
III.	CONCLUSION.....	32
IV.	REFERENCES	32

ABSTRACT

Due to an increase in the level of greenhouse gases counting carbon dioxide, one faces several changes in the environment together with global warming. Various approaches are put to the surface to help reduce carbon dioxide. Methods such as electrochemical, thermochemical, and photocatalysis are employed to amend the same. Each one of these has some pros and cons. This mini-review provides a brief discussion on the various cobalt-based catalysts that has been used over the years to help in Electrochemical CO₂ reduction (CO₂RR).

I. INTRODUCTION

Over the years, by virtue of industrial effluents and vehicle combustion, we find a rise in the number of greenhouse gases plus carbon dioxide. In May 2021, the CO₂ concentration was 419.13 ppm [1], directed to many environmental problems, including a rise in temperature, causing an imbalance in natural activities. At an individual level, one can help reducing amount of CO₂ in the atmosphere by growing more plants and soil amendment. However, this will not hold a significant contribution to reducing CO₂. Keeping this in mind, researchers have come up with methods to curtail the above problem by reducing CO₂ into species which is user friendly. However, CO₂ is a thermodynamically stable molecule with a firm double bond interaction between carbon and oxygen atoms having low Gibbs free energy so, to convert a non-reactive molecule to an energy-rich compound becomes challenging. Thus, requiring an external source to help in the same. Sources like heat, irradiation/photons, and electrons can be used [2]. Hence, methods like photochemical, electrochemical, biochemical, thermochemical, and radiochemical are listed (figure 1). Among these, electrochemical technique is promising towards the reduction accompanied with conversion of atmospheric CO₂ to products. As, the demonstration of this electrochemical method is simple, one can operate it with ease, it can function at neutral pH, ambient temperature and atmospheric pressure, with low energy utilization to produce valuable chemicals and fuels such as formic acid, methane, ethanol, and carbon using renewable electricity [1]. In this path, the first reaction noticed is breaking the C-O bond requiring colossal amount of electrical energy-giving carbon dioxide radical anion, following further conversion [3]. The different products obtained via the reduction of CO₂ include carbon monoxide, formic acid, methanol, methane, formaldehyde, oxalic acid, ethanol, etc. Insight on reduction potentials of the said compounds is of value when reducing CO₂ electrochemically, as it influences the thermodynamic accessibility of CO₂. What's more is that as the number of electrons transferred during electrolysis increases, the redox potential becomes more and more negative [4].



Thus, a large amount of energy is required to rearrange a linear CO₂ molecule to the bent radical CO₂⁻ structure. Also, the gathering of the nuclei to convert a simple molecule (CO₂) into a complex active molecule is challenging. On the other hand, when a high negative potential is utilized to the aqueous electrolyte solution, the Hydrogen Evolution Reaction begins to compete with CO₂ reduction reaction, since both the above reactions, occur at the same potential range, thus competing with each other resulting in decrease in faradaic efficiency. We find that the reduction of CO₂ into useful chemicals, encounter kinetic and thermodynamic challenges. Therefore, such electrocatalysts are necessary that suppress HER and enhance the selectivity of these chemicals [2].

At first, many electrocatalysts in addition to, Au, Ag, and Pd were used for CO₂RR facilitating, high electrocatalytic performances, selectivity, and stability with low overpotential, but were not cost-effective [1]. Later, transition metals like Iridium, Nickel, Iron, Ruthenium, Molybdenum, Copper, and Cobalt individually were employed to contribute as electrocatalysts for CO₂RR. These metals were in varied forms like a single atom, multi-metals, complexes, in the metal-organic framework (MOF), and oxides depending on their reactivity. Among these, Copper metal was the one that was frequently used in CO₂RR obtaining products like methane, ethylene, and other hydrocarbons. However, using Copper would yield not a single product instead multiple products making the process even more complex [5]. Among the transition metals Cobalt, (group VIII-B) has properties that include high catalytic performances, thermal stability, unique electronic features, high electrical conductivity, and chemical stability. Thus, making cobalt-based catalysts a promising material for CO₂RR applications. Cobalt, being bountiful is great alternative to noble metals like includes Pt, Ir, Ru [1]. Spinel-shaped Co₃O₄ is assured to be the most competitive candidate in the same. In this, Co²⁺ ions in tetrahedral sites and Co³⁺ ions in octahedral sites are observed [6]. It is perceived that Co₃O₄, though good in its performance has a very low intrinsic conductivity accompanied by slow rate of diffusion. To solve this one can, replace some of the Co²⁺ ions with another metal to obtain mixed metal oxides, thereby enhancing its performance.

Metal-nitrogen (M-N) active sites anchored within carbon material (M-N-C) provide easy electron transfer and more active sites for CO₂ [7]. Phthalocyanine compounds are known for their excellent electrocatalytic properties and, are well-known electrode modifiers since the 18 π conjugated skeleton with a strong π - π interaction in the structure facilitates electron mitigation from reactant to catalyst and vice versa. Cobalt phthalocyanine (CoPc) and its derivatives were found to be the most active [8].

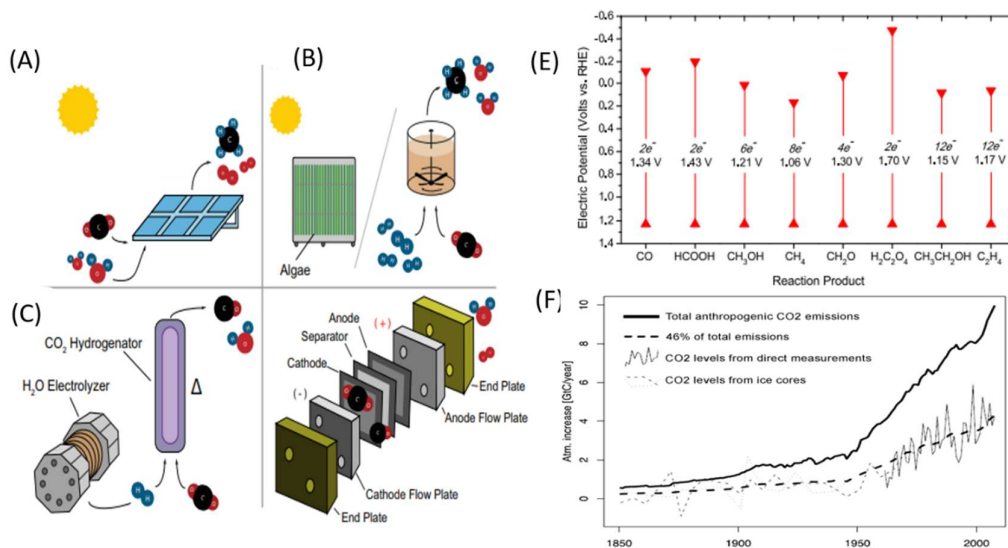


Figure 1. CO₂ conversion methods (A) photochemical and photoelectrochemical, (B) biochemical, (C) thermochemical, (D) electrochemical methods of producing syngas, alkanes, alcohols, or carboxylic acids from water and carbon dioxide, and (E) reduction potentials of small products. (F) CO₂ emissions vs CO₂ levels. Reproduced from reference [30] and <https://skepticalscience.com/co2-levels-airborne-fraction-increasing.htm>

Metal-organic frameworks (MOFs) being associated with larger organic porous materials also referred to as porous coordinating polymers or networks have a wide range of applications. MOFs are considered to have a highly porous structure, characteristic structural features, enormous surface area, and high conductivity. This hybrid material, is made up of three components namely metallic component, pore space, and the organic linker. The organic linkers are the sites that are attributed to the catalytic activity of the MOFs, making them an excellent choice for the adsorption, separation, and electro-reduction of CO₂ [2].

Loading transition metals onto carbon nanotubes (CNT) is also effective in CO₂RR.

Mostly KHCO₃ is used as an electrolyte during ERCO₂. It is observed that, when CO₂ is getting reduced, HER also takes place simultaneously at somewhat same potential. Thus, from the above two reactions one dominates the other. HER is the lowest among alkali metals including potassium and hence use of KHCO₃, as electrolyte is seen. Also, the cathodic reaction of CO₂ proceeds effectively with HCO₃⁻ as the solubility of HCO₃⁻ is more than CO₂ in an aqueous solution. Aqueous medium carried out reactions are useful, as they provide more valuable product compared to CO₂ reduction in the non-aqueous medium where oxalate, formate, and glycolate are produced [9].

This review, provides a summary of the research advancements, in regards to the use of Cobalt, may it be as a single atom or with multi-metal or in a complex. The synthesis, characterization, and few applications of cobalt-based catalysts for electrochemical reduction of CO₂ are studied.

II. SYNTHESIS, CHARACTERISATION AND ELECTROLYSIS

It was evident that electrochemical reduction of CO₂ (ERCO₂) was not easy due to some electrocatalysts not being selective towards CO₂ reduction, accompanied by HER. Thus, Singh et al. provided a method to check the activity of certain electrocatalysts towards ERCO₂ based on a half-cell test [9]. Initially, to synthesize cobalt oxide (Co₃O₄), Co (NO₃)₂ put to use as a precursor via polymer combustion route. Viscous gel was prepared using an aqueous solution (10 %w/w) of polyvinyl alcohol at 900°C, with constant stirring. PVA: Co ratio of about 3 was maintained by slowly adding an aqueous solution of 0.5 M Co (NO₃)₂ into the gel. The prepared solution kept overnight for drying at 80°C, resulting in a pink polymer matrix, which was later calcined at 600°C for 45 min to obtain a black coloured electrocatalyst. Using the prepared electrode, a half-cell study was carried out within a potential range of -3.0 to 2.0 v, in a 3-electrode cell assembly which comprised of Pt wire (counter electrode), Ag/AgCl (reference electrode), and cathode – Co₃O₄ (working electrode). The loading of Co₃O₄ was carried out on a gas diffusion layer, with cathode fed with CO₂ saturated KHCO₃ solution. Co₃O₄ was inactive in cyclic voltammetry (CV) (due to inter-conversion of Co²⁺/Co³⁺ oxidation states). Later based on current density, which is said to be related to the rate of the reaction, the electrocatalysts had to undergo three tests in 3 different electrolyte mediums (KHCO₃, KOH, DMF) at the same pH, in here Co₃O₄ was catalytically active during ERCO₂ giving formaldehyde with a yield of 417.9 ppm at -2.5 v [9]. XRD pattern (figure 2) shows Co₃O₄ diffraction peaks similar to the spinel structure of cobalt oxide (crystallite size of 29.55 nm). Two strong absorption bands at 660 and 580 cm⁻¹ seen from the FTIR spectrum of cobalt oxide confirmed the spinel structure of Co₃O₄. Due to the stretching-vibration mode, two Co–O peaks were observed. One band was observed at 660 cm⁻¹, with Co in a +2-oxidation state (tetrahedrally arranged), and the other band at 580 cm⁻¹ Co in a +3-oxidation state (octahedrally arranged) [9].

To get, a single liquid product, a two-electrode glass cell at different voltages was planned, by Yadav et al. to obtain, the optimum conditions to gain maximum Faradaic efficiency during ERCO₂, using Zn and Co₃O₄ as cathode and anode respectively. Zn and Co₃O₄, were synthesized by electrodeposition technique.[10] 0.1 M ZnCl₂.2H₂O and 0.1M Co (NO₃)₂.6H₂O solution were deposited separately on the surface of the graphite plate. For three whole minutes, 0.2 A of current was applied between the copper metal plate and graphite plate in an electrolytic cell to electrodeposit Zn. Later, acetone solution was used to remove deposited Zn and Co powder and heated at 100°C for 1 hour to obtain Zn powder [10]. Sodium and potassium carbonates together with bicarbonates were used as electrolyte solutions, and it

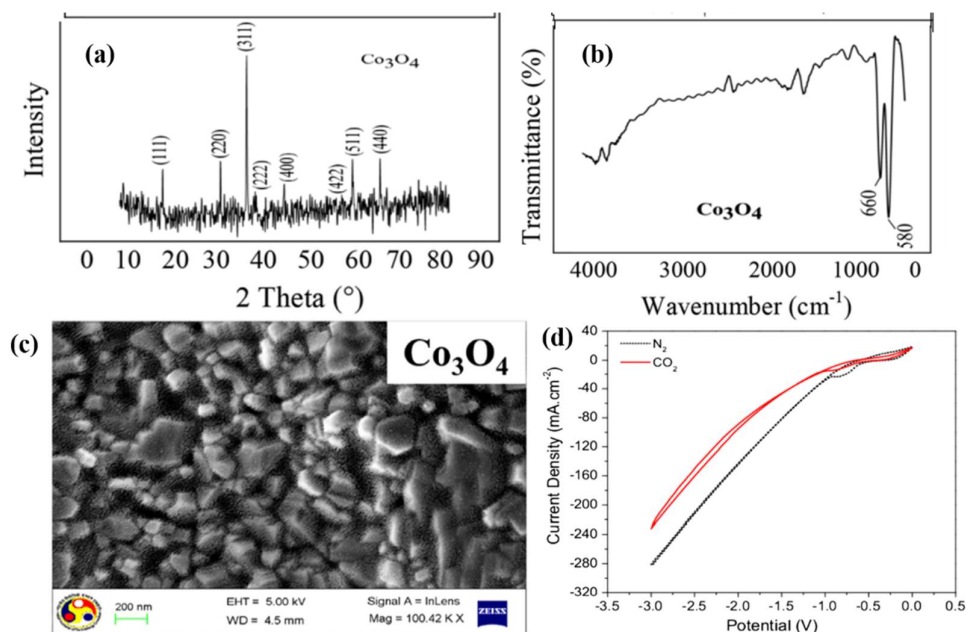


Figure 2: (a) XRD pattern; (b) FTIR spectra; (c) FESEM images and (d) Cyclic voltammograms, in the presence of CO_2 (solid line) and in inert (N_2) atmosphere (broken line) using electrocatalysts Co_3O_4 . Reproduced from reference [9]

was seen that, bicarbonate-based electrolytes showed high faradaic efficiencies (FE) than carbonate. FE of about 78.5% for HCOOH at 1.5 v potential in KHCO_3 electrolyte solution while using NaHCO_3 , FE was 64.7% at 2.5 v potential (a drop in FE caused due to high proton generation) [10]. They then, used the same principle this time by using Sn (cathode) and Co_3O_4 (anode) as an electrocatalyst. Here, Sn powder was prepared by electrodeposition. Additionally, graphite plates were in use, onto which the electrocatalysts were coated. ERCO_2 by this method resulted in the synthesis of HCOOH [5]. A similar methodology was used again by Yadav et al. This time by using CuO_2 as the cathode, producing ethanol as the major product at 2 v with small quantities of propanol, formic acid, methanol, formaldehyde, and acetic acid [3]. They then studied the effect of both Zn and Sn electrocatalysts as cathode and Co_3O_4 as anode towards Crystal violet dye removal and reduction of CO_2 to HCOOH using two different electrolytes, namely: KHCO_3 and NaHCO_3 solutions. It was viewed that, higher applied voltages were favourable for crystal violet removal, whereas low applied voltages would give high Faradaic efficiencies. High HCOOH faradaic efficiency of 45.3% was obtained in KHCO_3 electrolyte solution using Zn electrocatalyst at 2.3 v [11].

Thereafter, Shan Gao and co-workers prepared very thin, layers of Co_3O_4 and proved that the same increases ERCO_2 to many folds. Thus, ultrathin Co_3O_4 layers, which were prepared, by fast heating technique, with varied thickness was studied to produce formate [6]. At first 2D sheet-like structure with a sheet size larger than 500 nm was observed using TEM (figure 3a).

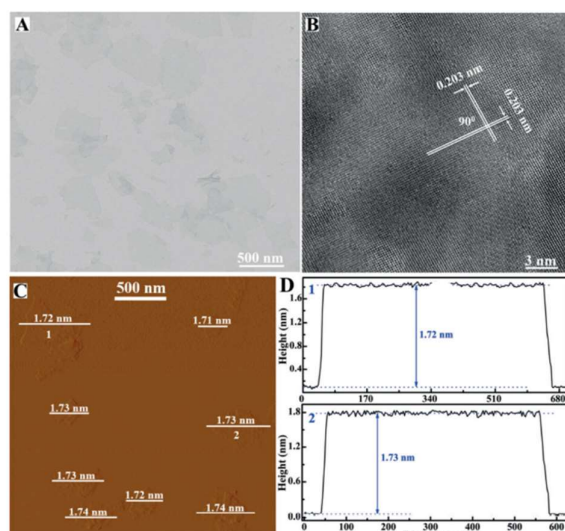


Figure 3. Characterizations for Co_3O_4 atomic layers with an average thickness of 1.72 nm. A) TEM image, B) HRTEM image, C) AFM image and D) the corresponding height profiles for Co_3O_4 atomic-layers with average thickness of 1.72 nm; the numbers 1 to 2 in (D) correspond to the numbers from 1 to 2 in (C). Reproduced from reference [6].

AFM (figure 3c) recorded the nearly transparent nature of the products implying their ultrathin thickness, and HRTEM (figure 3b) image revealed their [001] orientation, suggesting the formation of ultrathin Co_3O_4 layers with a highly preferred [001] direction [6]. A partially oxidized four-atom-thick cobalt layer was also fabricated (atomically thin layer) in 2016, which seemed to exhibit high intrinsic activity and selectivity towards formate production. The partial oxidation of the atomic layers could further improve the intrinsic activity, performing current densities of about 10 mAcm^{-2} over 40 h at -0.85 V versus SCE, with approximately 90% formate selectivity [12]. Shan Gao et.al. Then worked a lamellar inorganic-organic hybrid intermediate strategy was adopted to fabricate V_o -rich and V_o -poor Co_3O_4 single unit-cell layers. For this, synthesis of a lamellar $\text{Co}(\text{CO}_3)_{0.5}(\text{OH})_n - 0.11\text{H}_2\text{O}-\text{CTAB}$ hybrid using $\text{Co}(\text{acac})_3$ and CTAB via a self-assembly process was employed. Analysis of orderly mesostructured sample by small-angle X-ray diffraction pattern carried out at 180 C for 12 h. After 20 hours of reaction, the lamellar $\text{Co}(\text{CO}_3)_{0.5}(\text{OH}) - 0.11\text{H}_2\text{O}-\text{CTAB}$ hybrid found to gradually self-exfoliate into ultrathin $\text{Co}(\text{CO}_3)_{0.5}(\text{OH}) - 0.11\text{H}_2\text{O}$ layers, confirmed by XRD, TEM and AFM. Following a fast-heating process in distinct air and O_2 atmospheres resulted in the successful formation of single unit cell layers of Co_3O_4 at different concentrations of oxygen vacancies. Thus, working on cobalt single unit cells, he prepared different Co single cell unit layers with a varied amount of Oxygen vacancies (V_o), and later observed that the more the oxygen vacancies in Co_3O_4 single-unit cell (-0.87 v , faradaic efficiency of 87.6%) the more is the CO_2 adsorption resulting in increased formate production. This, was explained by studying its potential-dynamic electrochemical behaviour [13]. Using linear sweep

voltammetry (LSV), large peaks were observed, showing its contribution to catalytic reduction of CO₂. V_o-rich Co₃O₄ single-unit-cell layers exhibited a current density of 2.7 mAcm⁻² at -0.87 V versus SCE, which was two-times as large as that of the V_o-poor Co₃O₄ single-unit-cell layers. To quantify liquid and gas products by ¹H nuclear magnetic resonance, gas chromatography analysis, and stepped potential electrolysis was carried out, revealing that the V_o-rich Co₃O₄ single-unit cell layers possessed a maximum faradaic efficiency of 87.6% for producing formate at potential of -0.87 V versus SCE. However, the V_o-poor Co₃O₄ single-unit-cell layers showed a faradaic efficiency of 67.3%. Also, V_o-rich Co₃O₄ single-unit-cell layers showed negligible decay in the steady-state current density while V_o poor Co₃O₄ were stable only for a short time [13]. Figure 4 displays the preparation strategy, TEM, HRTEM, and AFM of V_o-rich and V_o-poor Co₃O₄.

Huazhang Zhao and co-workers presented a new technique to produce formic acid using a Microbial Electrolysis Cell (MEC) driven by a Microbial Fuel Cell (MFC). In MFC, microorganisms are used to capture energy as bio convertible substrates in the form of electricity. However, low voltage generated by MFC (less than 0.8 V) could not fulfil the low potential requirement in conventional ERCO₂. The complication was taken care of, by using MEC at the base of MFC. First, by ultrasonication technique, the active MWCNTs and CoTAPc were dispersed in DMF solvent separately for one hour, obtaining a consistent

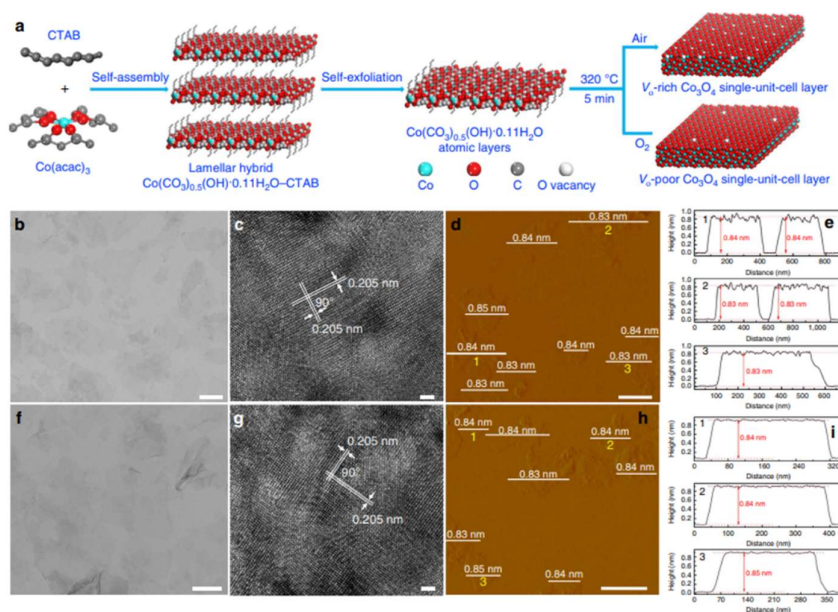


Figure 4: Preparation and characterization for the V_o-rich and V_o-poor Co₃O₄ single-unit-cell layer. (a) Scheme for the formation of V_o-rich and V_o-poor Co₃O₄ single-unit-cell layer, respectively. Characterization for the V_o-rich Co₃O₄ single-unit-cell layer: (b) TEM image, (c) HRTEM image, (d) AFM image and (e) the corresponding height profiles; the numbers from 1 to 3 in d correspond to the numbers from 1 to 3 in e. Characterization for the V_o-poor Co₃O₄ single-unit-cell layer: (f) TEM image, (g) HRTEM image, (h) AFM image and (i) the corresponding height profiles; the numbers from 1 to 3 in i corresponding to the numbers from 1 to 3 in h. The scale bars in b-d and f-h is 250, 1, 500, 200, 1 and 500 nm, respectively. Reproduced from reference [13]

solution known as MWCNT-DMF and CoTAPc-DMF, respectively. To construct multilayer films on substrate electrodes, both indium tin oxide (ITO) and graphite electrode (GE) were immersed in an aqueous solution of positively charged PEI ($10 \text{ mg}\cdot\text{mL}^{-1}$) for 30 min and then rinsed with water and dried under an N_2 gas flow. On the other hand, the positively charged PEI-precoated substrate was alternately dipped in the negatively charged MWCNT-DMF and positively charged, CoTAPc-DMF for 30 min, respectively. In doing so repeatedly, films with desired multiple layers were obtained, marked as ITO-(MWCNT/CoTAPc) $_n$ or GE-(MWCNT/CoTAPc) $_n$ ($n = 1-5$). Later, MEC used a biological anode, instead of a common electrode, on to which the substrate was oxidized by bacteria. Electrons generated at anode were transferred, to cathode via an external circuit, while proton generated were diffused through a proton exchange membrane to the cathode. Finally, these electrons and protons participated in the reduction reactions at the cathode. MEC would then generate hydrogen or methane under much smaller voltage than that needed for common electrolytic reactors. Figure 5e displays the schematic representation of ER CO_2 by using MEC and MFC with the mechanism of reduction of CO_2 to HCOOH . It was observed that, introduction of Carbon Nano Tubes (CNTs) to the cobalt tetra-amino phthalocyanine (CoTAPc) modified electrodes by reducing the overpotentials. Therefore, Multi Walled Carbon Nano Tubes (MWCNT) and CoTAPc composite electrode, were fabricated using layer-by-layer (LBL) self-assembly technique, this was used, as the MEC cathode for CO_2 reduction to formic acid. CO_2 was electro-reduced in

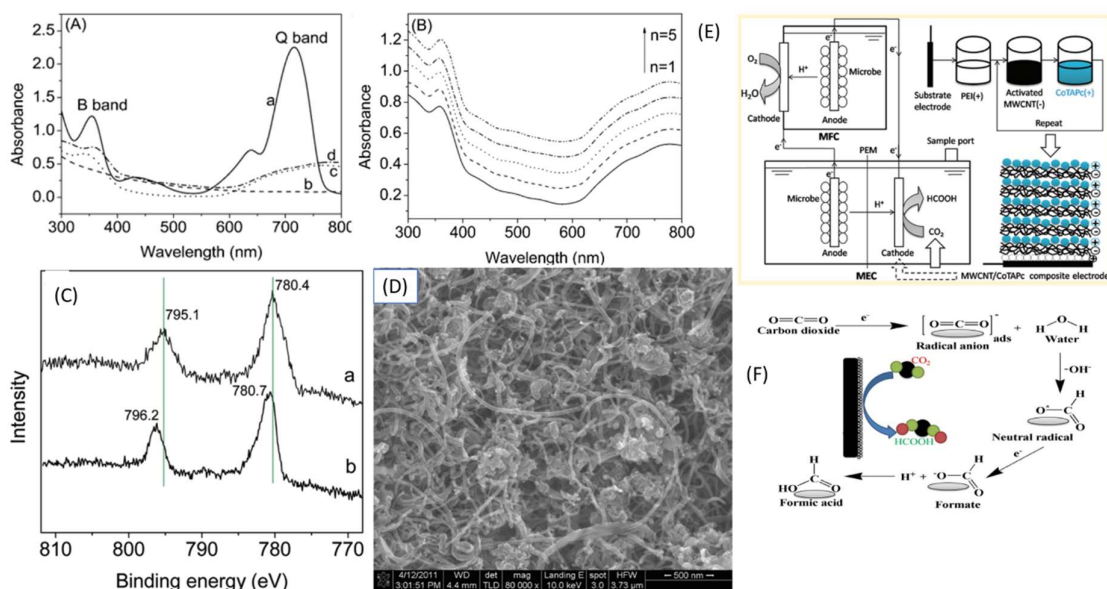


Figure 5: UV-vis spectra of 10^{-5} M CoTAPc in DMF solution (a), ITO-MWCNT (b), ITO-CoTAPc (c), and ITO-(MWCNT/CoTAPc) $_n$ electrodes (d) electrodes (A) and ITO-(MWCNT/CoTAPc) $_n$ electrodes (B). SEM image (D) of the ITO-(MWCNT/CoTAPc) electrode and XPS spectra (C) of Co_{2p} on the ITO-CoTAPc (a) and ITO-(MWCNT/CoTAPc) electrodes (b). schematic CO_2 RR using MFC, MEC (E) Proposed mechanism for reduction of CO_2 to HCOOH (F) Reproduced from [8] and [10]

the cathodic chamber of the MEC. Compared with the electrode modified by CoTAPc alone, the MWCNT/CoTAPc composite modified electrode could increase the current and formic acid production rate by approximately 20% and 100% [8]. Existence of phthalocyanine ring was observed, peculiar to B and Q bands from UV-vis spectra (figure 5) of the CoTAPc-DMF solution. Spectra, of ITO-CoTAPc (figure 5A, c) and ITO-(MWCNT/CoTAPc) (figure 5A, d), displayed in B and Q bands were broadened and weakened, due to aggregation of CoTAPc on the modified electrodes. Concerning ITO-CoTAPc spectra, redshifts for B and Q bands appeared in the spectra of ITO-(MWCNT/CoTAPc). This was observed due to electron transfer from phthalocyanine ring to MWCNTs, causing expansion of the macrocyclic conjugated structure of CoTAPc and reduction in energy level difference between the highest occupied molecular orbital (HOMO) and the lowest unoccupied molecular orbital (LUMO). The multiple-layer alteration promoted the catalytic effect of the modified electrodes owing to the increase of MWCNTs and CoTAPc in the modification films, the absorbance of modified electrodes increased, concluding that the interaction of MWCNTs and CoTAPc is beneficial [8].

Aoi et al. reported a method in which CO₂ reduced to CO in water. Here, cobalt (II) chlorin complex was adsorbed on MWCNT (in water) giving Co(II)(Ch)-modified electrode, as this experiment required the binding of CO₂ to the Co(I) complex to produce CO, two electron reduction was needed to be carried out from Co(I) complex using CO₂. It was seen that, the π - π interaction between MWCNT and Co(II)(Ch) provided a hydrophobic environment to bind with CO₂ rather than a proton. Therefore, the same, was taken care of by selectively catalysing CO₂ to CO in H₂O (pH = 4.6) at an applied potential of -1.1 V vs. NHE with a high faraday efficiency of 89% [14].

Meng Zhu and co-workers, proposed a catalytic mechanism, that not only reduced CO₂ electrochemically, but also helped in the degradation of 4-nitrophenol by electrocatalysis, and Advanced Oxidation Processes (AOP), using Co₃O₄@C as anode and SnO₂/CC as cathode. During this process, 3D gear-shaped Co₃O₄@C anodes were prepared for degradation of 4-nitrophenol, and Co₃O₄ electrodes were synthesized, using 0.1, 0.3, 0.5, and 0.7 g urea called Co0.1, Co0.3, Co0.5, and Co0.7, respectively in which the amount of urea did not change the crystallinity of Co₃O₄. As shown in figure.5, the amount of urea had a great influence on the morphology of Co₃O₄ [15]. It was noted, that with an increase in the concentration of urea, the hollow structure of Co₃O₄ gradually filled. When the amount of urea increased to 0.7 g, the Co₃O₄ showed a 3D-hexagonal morphology decorated with some nanoparticles. SnO₂/CC was

prepared hydrothermally, having a uniform morphology. SnO₂ nanosheets were grown on the carbon cloth (thickness of ~20 nm) facilitating more active sites for electrochemical reduction of CO₂. Co₃O₄@C and SnO₂/CC both as anode and cathode respectively, in the presence of peroxy-mono-sulphate (PMS) were used to achieve removal of 4-nitrophenol (4-NP) and simultaneous electrocatalytic reduction of CO₂ [16].

Owing to proprieties displaying energy storage and adsorption capacity with high chemical stability and excellent conductivity, cost-effective materials like carbon nanotubes, graphene, mesoporous carbon, and Carbon Nano Fibres (CNFs) are among the most occupying and anticipating materials. CNFs being flexible, can tune the given structure. Nousheen Iqbal and co-workers studied the characteristics of carbon, and developed a facile in situ technique, where flexible CNF membranes were synthesized and embedded with Co₃O₄ Nano Particles (NPs) via electrospinning and carbonization treatment. CNFsCo hybrid membranes were prepared, by modifying the relative quantity of cobalt acetylacetonate Co(acac)₂ in the precursor solution. In order increase the electrical conductivity, carbonizing PAN nanofibers at high temperatures was performed on the CNFs matrix. Precursor fibres were initially dried at 70°C for 1h under vacuum to eliminate the solvent and then sustained in an oven for 2 h at 280°C. Acquired nanofibrous membranes were then annealed at 850°C for 2 h with a heating amount of 2°C min⁻¹ under N₂ flow in a tube furnace, forming a smooth and flexible membrane [17].

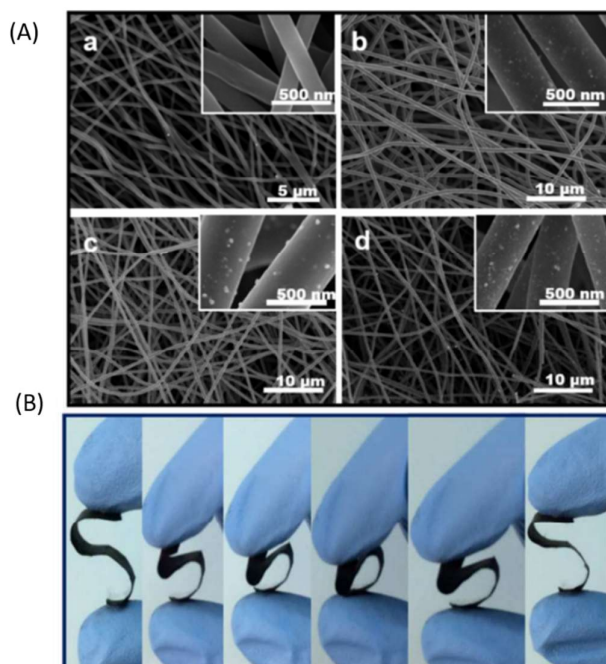


Figure 6, A) FE-SEM images of CNFs with different salts contents of (a) 0, (b) 2, (c) 3, and (d) 4 wt.%. (B) Digital images presenting the robust flexibility of CNFs-Co-4 membranes. Reproduced from reference [17]

Apart from CNFs-Co, other samples like CNFs-Co-2, CNFs-Co-3 and CNFs were made ready by using 1 g, 1.5 g and 0 g of $\text{Co}(\text{acac})_2$ for comparison, in the precursor sol, respectively. FE-SEM images (figure 6) of the CNFs-Co composites with different Co_3O_4 loadings implied that the obtained nanofibers were haphazardly arranged as three-dimensional (3D) open-cell nonwoven membrane geometry. From the fibre diameter of the CNFs- Co-4, CNFs-Co-3, and CNFs-Co-2 being 674, 743, and 796 nm, respectively, it's noticed that with the insertion of salt in composites, there was an increase in net charge density followed by a decrease in fibre diameter, both increasing conductivity of spinning solutions. High-magnification SEM images of surface and cross-section of Co_3O_4 doped CNF displayed that Co_3O_4 NPs were not only consistently spread out on the surface of the CNFs, but also ingrained into the CNF framework (seen from a cross-section of Co_3O_4 doped CNFs), in this way CNFs provide a huge surface area for the electrolyte [17].

Among the family of macrocyclic pentadentate (N5 ligands), Bonin et al. discovered that the Co^{2+} complex and the Fe^{3+} complex was active towards CO_2 reduction at the carbon electrode, with cobalt catalyst producing CO while formic acid was obtained from the iron analogue. $[\text{Co}(\text{II})\text{L}]^+$. Catalysis eventuated, after two-electron reduction (the first electron is located on the metal centre while the second is borne by the ligand). 1-hour electrolysis experiment at -1.26 V vs. SHE, led to the formation of CO exclusively with 82% faradaic yield, a current density of 0.4 mAcm^{-2} , and an overpotential of ca. 570 mV. In the course of long-term electrolysis (several hours later), deactivation of the catalyst occurred [18].

A hetero-junction proto-type, by the name - $\text{Co}_3\text{S}_4@ \text{Co}_3\text{O}_4$ core-shell, octahedron structure was proposed by Yan et al. via hydrothermal lattice anion exchange protocol to device the electrochemical reduction of oxygen and carbon dioxide with high performance. Here 0.6 mmol of $\text{Co}(\text{NO}_3)_2$ and 0.15 mmol of PPh_3 were evenly dissolved in 40 mL of deionized water with constant stirring, followed by slowly adding ammonia solution (28%) into the above mixture at 7.6 pH, then transferred into a 50 mL autoclave, sealed at 180°C for 24 h. The sample obtained was then rinsed, centrifuged, dried, and went through inert annealing for 2 h at 500°C under an argon flow. Co_3O_4 octahedrons were later coated, via lattice anion exchange method by scattering prepared sample in 40 mL 0.5 M Na_2S and hydrothermally autoclaved at 120°C for 24 h. On cooling, the products were centrifuged, rinsed, and vacuum dried at 80°C overnight. Co_3S_4 nanoneedles were synthesized to compare. For electrolysis, A bi-functional catalyst, consisted of a p-type Co_3O_4 core and n-type Co_3S_4 shell, which supplied high surface electron density with high capacitance, without sacrificing mechanical robustness. A four-

electron Oxygen Reduction Reaction (ORR) process, identical to the Pt catalysed Oxygen reduction reaction, is validated using the core-shell octahedron catalyst. The synergic interaction between cobalt sulphide and cobalt oxide bi-catalyst reduced the activation energy to convert CO₂ into adsorbed intermediates and in this way, enabled CO₂ reduction reaction to run at a low overpotential, with formate as the highly selective main product at a high faraday efficiency of 85.3%. Co₃S₄@Co₃O₄ core-shell octahedrons synthesized, were then used in supercapacitors, ORR, and carbon dioxide reduction reactions [19]. The selected area electron diffraction (SAED) pattern (figure 7I) displayed the hexadic form of the sample. O being located at the core, while S is distributed on the surface shell involving the terrace, edge, and corner (figure 7J), all this was observed using the energy-dispersive X-ray spectroscopy (EDX) [19].

Aljabour et al. examined the catalytic behaviour of semi-conducting Co₃O₄ nanofibers catalyst for CO₂ conversion to CO. They synthesized an electrocatalyst, just by mere expansion of the electrode network with Nano-fibrous interconnection, thereby carrying out the electrosynthesis of CO without using any other metal. In their work poly-acrylonitrile (PAN) as a polymer template, was used to give a high crystalline Co₃O₄ fibre [20]. SEM of the same in figure 6.

Co₃O₄ though abundant and available at low cost, its electrochemical performance is limited by the intrinsic disadvantage of poor electrical conductivity. It is also observed that Silver (Ag) being at a low cost is selective towards CO during ERCO₂. Hence in-cooperating with this element in Co₃O₄ could enhance the catalytic property of the electrode. At nanoscale, Metal-

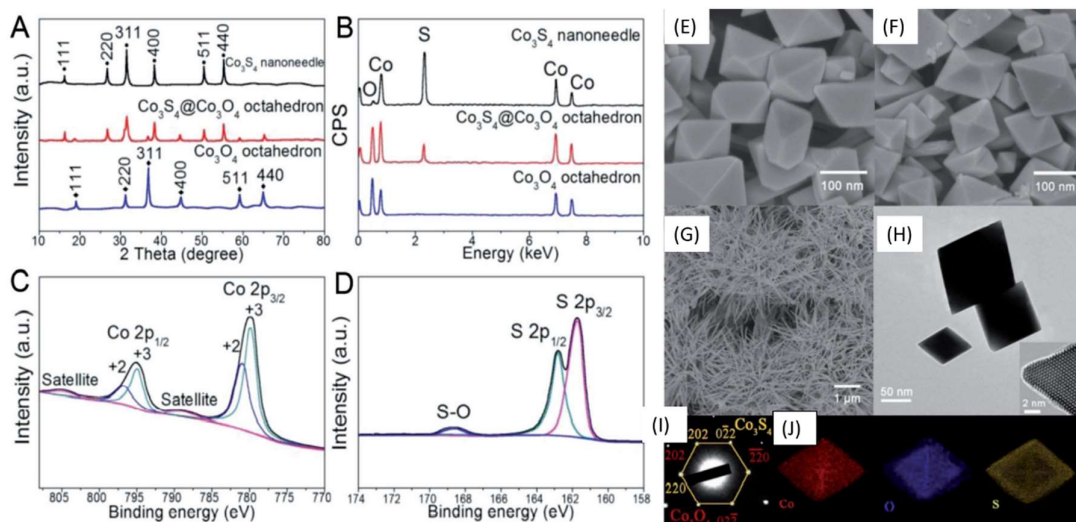


Figure 7: A) XRD of Co₃O₄ octahedrons (blue), Co₃S₄@Co₃O₄ octahedrons (red), and Co₃S₄ nanoneedles (black), B) EDX spectra of Co₃O₄ octahedrons (blue), Co₃S₄@Co₃O₄ octahedrons (red), and Co₃S₄ nanoneedles (black), C) XPS spectra of Co 2p level on Co₃S₄@Co₃O₄ octahedrons, and D) XPS spectra of S 2p level on Co₃S₄@Co₃O₄ octahedrons. FESEM image of E) Co₃O₄ octahedrons, F) Co₃S₄@Co₃O₄ octahedrons, and G) Co₃S₄ nanoneedles, H) TEM and HRTEM of Co₃S₄@Co₃O₄ octahedrons, I) SAED pattern of Co₃S₄@Co₃O₄ octahedrons, and J) EDX elemental mapping of Co₃S₄@Co₃O₄ octahedrons. Reproduced from [19]

organic frameworks (MOF) can be used, in drug delivery, sensor, gas storage, and catalysis. Having a central metal ion and organic ligand form a three-dimensional crystalline compound. MOF can work as a heterogeneous catalyst by observing the intrinsic oxidation-reduction activity of the central metal ion. Zhang et al., therefore, proposed a novel mixed metallic Metal-organic framework (MOF), $[Ag_4Co_2(py_z)PDC_4][Ag_2Co(py_z)_2PDC_2]$ which transformed Ag into Ag-doped Co_3O_4 catalyst, exhibiting excellent electrocatalytic performance for reduction of CO_2 in water to syngas ($H_2 + CO$). Stirring 1 mmol $AgNO_3$ (0.170 g), 1 mmol $Co(NO_3)_2 \cdot 6H_2O$ (0.291 g), 1 mmol PDC (0.167 g), and pyz (1 mmol, 0.08 g) in 25 mL Teflon-lined stainless steel autoclave, with 7 mL H_2O was 1st done followed with heating the same at 160 °C for five days. The product was then rinsed using deionized water thrice and then dried in an oven at 60 °C overnight to get $[Ag_4Co_2(py_z)PDC_4][Ag_2Co(py_z)_2PDC_2]$ purple crystal (Ag/Co-based MOFs). By tempering the above product in the air at 350 °C for 4 h with a heating temperature rate of 2 °C min^{-1} , then cooled, black powder of Ag/ Co_3O_4 was obtained. On the other hand, black powder of Co_3O_4 was obtained by dissolving 2 mmol $Co(NO_3)_2 \cdot 6H_2O$, 4 mmol NH_4F , 5 mmol urea, and 20 mL H_2O in a 25 mL Teflon-lined stainless steel autoclave, with continuous stirring. Later heated for 12 h at 100°C, followed by washing the sample using deionized water, and drying overnight at 60 °C resulting in formation of a pink powder which turned black after calcinating the sample at 350°C in the air for 4 h with a rate of 2°C per min. The same gives faradaic efficiency up to 55.6 %. Ag was found to inhibit the production of H_2 and so making Ag improve the efficiency of CO. Thus, a novel Ag/Co-based mixed-metal MOF was obtained via the hydrothermal method, which was then calcined at high temperature to get porous Ag/ Co_3O_4 nanomaterial, and used electrode for $ERCO_2$ [21]. Ag and Co_3O_4

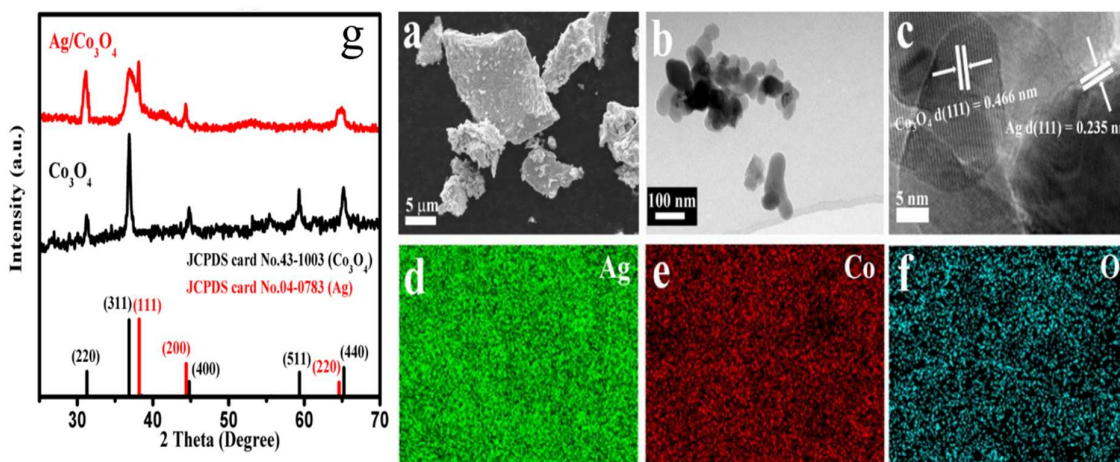


Figure 8: (a) SEM image of Ag/ Co_3O_4 material; (b) TEM and (c) HRTEM images of Ag/ Co_3O_4 material; EDS elemental mapping images of Ag, Co and O. g) PXRD pattern of the Co_3O_4 and Ag/ Co_3O_4 samples. Reproduced from [21]

were well mixed, as seen from TEM and HRTEM images. EDS imaging concluded uniform distribution of Ag, Co, and O elements in the sample (figure 8) [21]. An approximately similar procedure was followed by embedding gold (Au) in Co_3O_4 , giving nanowire arrays of beaded $\text{Au}@ \text{Co}_3\text{O}_4$ (denote as $\text{Au}@ \text{Co}_3\text{O}_4$ NAs). $\text{Co}(\text{OH})_2$ NAs on Cu foam, sonication of Cu foam in 3 M HCl for approximately 30 min was done to take off copper oxide layer on surface, later rinsed with water and ethanol, and then dried in the air. 2.86 mmol $\text{Co}(\text{NO}_3)_2 \cdot 6\text{H}_2\text{O}$, 5.79 mmol NH_4F and 14 mmol $\text{CO}(\text{NH}_2)_2$ were dissolved in 20 mL H_2O , stirred and subsequently transferred to a Teflon-lined stainless steel autoclave. Cu foam ($1 \times 2 \text{ cm}^2$) was then dipped in this solution and kept at $120 \text{ }^\circ\text{C}$ for 9 h in an oven. $\text{Co}(\text{OH})_2$ nanoarrays formed were then rinsed in water and dried. Afterwards $\text{Co}(\text{OH})_2$ NAs was immersed in an autoclave containing a solution of 20 mmol 2-MIM in 5 mL of water and ethanol for 12 h at 85°C then cooled. Later washed with water and dried, forming beaded ZIF-67 NAs on Cu foam. By annealing the above sample in air at $350 \text{ }^\circ\text{C}$ for 4 h in furnace with a heating rate of $1 \text{ }^\circ\text{C min}^{-1}$, beaded Co_3O_4 NAs electrode was synthesised, which was added in a mixture of 0.1 mL pyrrole and 30 mL ethanol for 12 h and dried. Later HAuCl_4 (0.2 g/L) solution was added to the same in the dark to procure the beaded $\text{Au}@ \text{Co}_3\text{O}_4$ NAs. During electroreduction, $\text{Au}@ \text{Co}_3\text{O}_4$ NAs not only converted CO_2 to syngas but also performed oxygen evolution reaction with an overpotential of 320 mV and current density of 50 mAcm^{-2} , demonstrating that loaded Au serves as a conductive network to promote the rate of electron transport. It was observed that, the introduction of Au

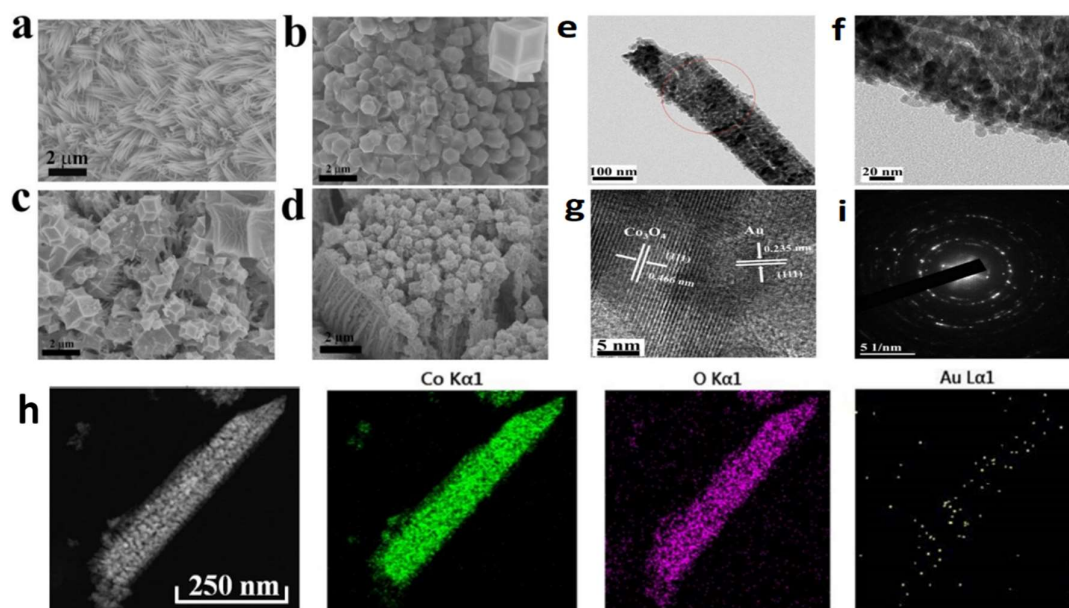


Figure 9: SEM images of (a) $\text{Co}(\text{OH})_2$ NAs; (b) ZIF-67 NAs; (c) Co_3O_4 NAs; (d) $\text{Au}@ \text{Co}_3\text{O}_4$ TEM (e and f), HRTEM images (g) and the SAED pattern (i) of $\text{Au}@ \text{Co}_3\text{O}_4$ NAs, (h) TEM images and the corresponding EDX mapping of Co, O and Au in $\text{Au}@ \text{Co}_3\text{O}_4$ NAs. Reproduced from [22]

nanoparticles could reduce the electron density around Co in Co_3O_4 NAs, which was favourable for providing more catalytically active sites also, the 3D composites structures $\text{Au}@\text{Co}_3\text{O}_4$ NAs facilitated the delocalization of the Co-O bond strengthening the catalytic activities. Furthermore, the doping of Au optimized the adsorption of Gibbs free energy of intermediates in the catalytic process to improve the catalytic activity [22]. The SEM (figure 9a) image of $\text{Au}@\text{Co}_3\text{O}_4$ NAs in harmony with Co_3O_4 NAs exhibited $\text{Au}@\text{Co}_3\text{O}_4$ NA being unchanged after immersion in the HAuCl_4 solution. EDX spectrum (figure 9h) of $\text{Au}@\text{Co}_3\text{O}_4$ NAs affirmed the presence of Au, Co and O elements, displaying that Au and Co_3O_4 were concurrent in $\text{Au}@\text{Co}_3\text{O}_4$ NA [22].

Later, Seongmin Park and co-workers used a method portraying fast electrode kinetics, high efficiency and decreased load, of electrical energy, compared to other methods known as Solid oxide electrolysis cell (SOEC), an effective CO_2 conversion method by electrolyzing CO_2 to CO. For this, Perovskite $\text{La}_{0.6}\text{Sr}_{0.4}\text{Co}_{0.7}\text{Mn}_{0.3}\text{O}_3$ (LSCoMn) was developed from metal precursors of $\text{La}(\text{NO}_3)_3 \cdot 6\text{H}_2\text{O}$, $\text{Mn}(\text{NO}_3)_2 \cdot 6\text{H}_2\text{O}$, $\text{Co}(\text{NO}_3)_2 \cdot 6\text{H}_2\text{O}$, $\text{Sr}(\text{NO}_3)_2$ using sol-gel technique. All of this dissolved in distilled water, followed by the addition of EDTA (99.5%) and citric acid (99.5%) as chelating agents with the molar ratio of metal ions/citric acid/EDTA to 1:1.5:1. Later by adding ammonia water, the pH was adjusted to 7 and stirred at 90°C until the solution was set as gel which was further dried at 200°C for 1 h under air, then preheated at 700°C for 10 h to remove the organic components. Black powder of sample was obtained by pulverizing the above-prepared product followed by calcinating at 1100°C for 10 h in air. Co-R.P.LSCoMn was later synthesized in the same way by sol-gel technique and calcinated at 1350°C . Ceramic-based materials in forms of perovskites were used as cathode catalysts, as they are highly stable under electrochemical redox condition and coking resistance despite their relatively low catalytic activity. Active Ruddlesden-Popper material with a mechanism of in situ exsolution of Co nanoparticles revealed a good reversibility of structural transition between the Ruddlesden-Popper and the perovskite structure during reaction cycles. During electrolysis, a current density of 630 mA/cm^2 accomplished at a voltage of 1.3 v and temperature of 850°C with a very high Faraday efficiency of 95% or larger. By galvanostatic stability test it was seen that there were no signs of degradation, implying that the Ruddlesden-Popper structure was highly robust as the cathode catalyst for the CO_2 electrolysis. Weight change of the catalyst material with temperature was measured using TGA (figure 10) to check the phase transition temperature of Co-R.P.LSCoMn and the number of oxygen vacancies formed around the reaction temperature of CO_2 electrolysis. As the temperature increased, the weight of the

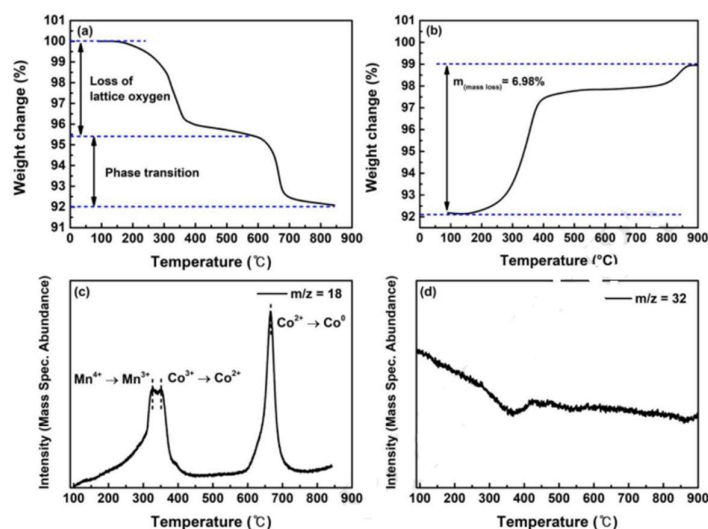
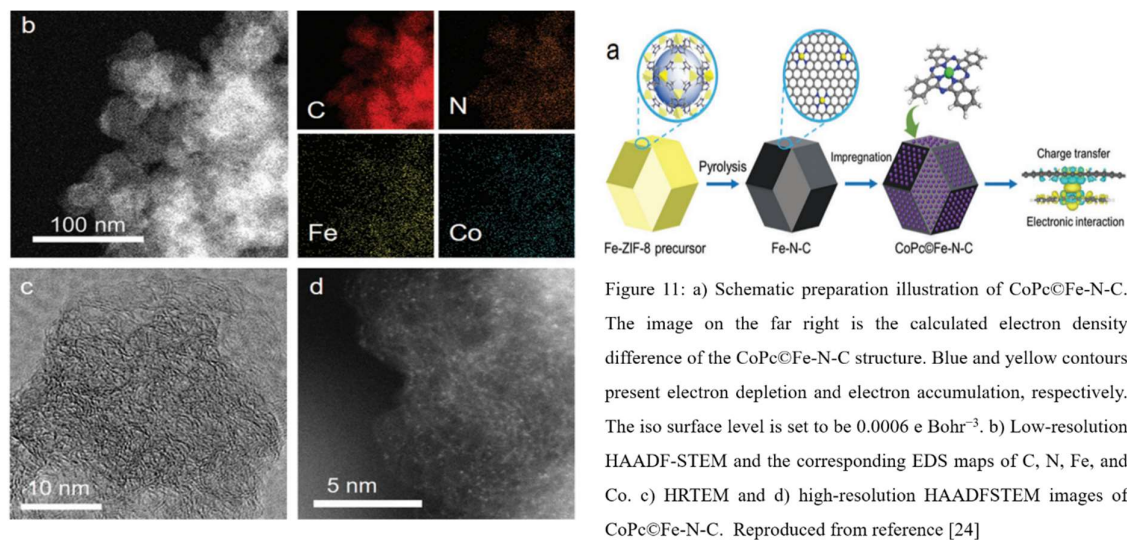


Figure 10: Thermogravimetric analysis (TGA) of (a) LSCoMn in the 20% H₂/N₂ condition and (b) CoR.P.LSCoMn in the air condition at temperature range of 90 - 850 °C. (c) H₂-TPR profile for the LSCoMn and (d) O₂-TPO profile for Co-R.P.LSCoMn catalyst at temperature range of 90 - 850 °C. Reproduced from reference [23]

catalyst decreased due to oxygen loss from the lattice. Between 600 °C and 700 °C, catalyst weight decreased drastically, denoting that phase transformation took place on the Ruddlesden-Popper structure with the exsolved Co metal nanoparticles. However, by re-oxidation of Co metal to Co₃O₄, the weight loss of the Co-R.P.LSCoMn recovered as the temperature in the air increased [23].

Metal–nitrogen active sites anchored within porous carbon (M-N-C) have been identified as a new class of efficient CO₂RR catalysts. Long Lin and co-workers developed a synergistic catalysis strategy to enhance the CO₂RR performance by anchoring Fe-N sites with cobalt phthalocyanine (CoPc) (denoted as CoPc@Fe-N-C) by using a sequential pyrolysis and post-impregnation method. CoPc@Fe-N-C was coalesced by two steps: pyrolyzing ammonium ferric citrate-functionalized ZIF-8 nanoparticles in Ar at 1000°C for 4 h to prepare Fe-N-C, there-after to obtain CoPc@Fe-N-C, Fe-N-C was saturated with CoPc dissolved in N, N-dimethylformamide solution. Compared with Fe-N-C, the onset potential of CO₂RR was as low as -0.13 v versus RHE, maintained over CoPc@Fe-N-C. Faradaic efficiency above 90% was significantly broadened from 0.18 to 0.71 V, accompanied with a maximum tenfold increase in CO, current density and enhanced stability. Density functional theory calculations revealed that the CO desorption, was greatly promoted, and the competitive HER was suppressed effectively over CoPc@Fe-N-C. Though HCOOH formation remained unchanged. High-resolution TEM (HRTEM) and high-angle annular dark field-scanning transmission



electron microscopy (HAADF-STEM) (figure 11) images reaffirmed that metallic-single atoms are solely secured within the porous carbon, portraying uniform distribution of CoPc and Fe-N sites in CoPc@Fe-N-C [24].

Lately, Zhichao Miao and co-workers designed a method to introduce Zn to a Co-based zeolitic imidazolate framework (ZIF-67) like this, presenting a Zn modified Co@N-C composites. In the attempt to slow down the aggregation of Co species, direct annealing process of Zn species was used, and studied with different Co/Zn ratios and pyrolysis temperatures. Sum of 1.55 mmol of concentration of the two, $\text{Co}(\text{NO}_3)_2 \cdot 6\text{H}_2\text{O}$ and $\text{Zn}(\text{NO}_3)_2 \cdot 6\text{H}_2\text{O}$, dissolved in 3 mL of water and then added to 20 mL of 2-methylimidazole (5.5 g). The same stirred at room temperature for 6 h. Later the supernatant was poured out by centrifugation, with lower precipitate being collected and washed thrice with methanol, which was then dried in a vacuum oven at 70°C overnight. The obtained product was calcined in an N₂ atmosphere with a heating rate of 1°C/min, at 800 °C, for 4 h. The gotten composites are denoted as Zn-Co@N-C-X [X stands for the Co content ($X = a/(a+b)$)]. Zn-Co@N-C-25 treated at different temperatures is named Zn-Co@N-C-25-Y, where Y stands for the final pyrolysis temperature (600, 700, 800, 900, and 1000 °C). Through this it was observed that, with an increase in Zn contents, the textural properties gradually improved, which can be due to the introduction of Zn species delaying the aggregation of Co species and decreasing the contents of graphitic carbon. Thus, Zn species promote hierarchical porosity, which might offer plenty catalytic active sites and favour mass and charge transport. Due to the pyrolysis of imidazolates, the specific surface area gradually improved as the temperature raised from 600 to 900°C. The FE(CO)% of Zn-Co@N-C gradually improved from 25% to 60%, current density also improved from 1.8 to 4.2

mAcm^{-2} , so also no evident decreases existed in current density and $\text{FE}(\text{CO})\%$ after 40 hours, showing the prominent electrochemical stability of Zn-Co@N-C catalyst [7]. XRD technique was applied to assess the crystal structure of Zn-Co@N-C-X composites. As demonstrated in Fig. 12 (a) exhibits, characteristic peaks of metallic Co species and the diffraction peaks at 44, 55, and 76° were ascribed: (111), (200), and (220) reflections. Proposing that the homogeneously distributed Co species in the Zn-Co-ZIF materials were reduced and aggregated to metallic particles in the pyrolysis process. With the introduction of Zn species, the peaks of the Co phase became weak and broad, displaying smaller particle sizes with higher Zn contents. Thereby implying that Zn species inhibit the aggregation of metallic Co species. Fig. 12 (b) compares the XRD patterns of Zn-Co@N-C-25 at different pyrolysis temperatures. With the temperature enhancing from 600 to 800 $^\circ\text{C}$, the intensity of diffraction peaks, owing to metallic Co species, increases slightly, and the crystalline size slowly increases from 3.69 to 6.90 nm. However, with the temperature reaching 900 and 1000 $^\circ\text{C}$, the diffraction peaks sharply enhance and the crystalline size increases to 18.4 and 28.3 nm, implying the gathering of metallic Co species to large particles. Therefore, the pyrolysis temperature has an extensive influence on Co particle size [7].

Numerous materials like metals and their oxides, alloys, transition metal complexes, molecules, chalcogenides, and carbon-based materials have been tested and used as electrodes for CO_2RR . Among these, nitrogen anchored metal atom (M-NX) moieties, a single-atom metal material, owing to its theoretically maximized atomic utilization and peculiar electronic structure, has been considered an outstanding electro-catalyst for CO_2RR in aqueous solution. However, M-NX electro-catalysts are mostly powder-based. For this reason, polymer binders such as nafion, are always employed to make these catalysts useful as working electrodes [25].

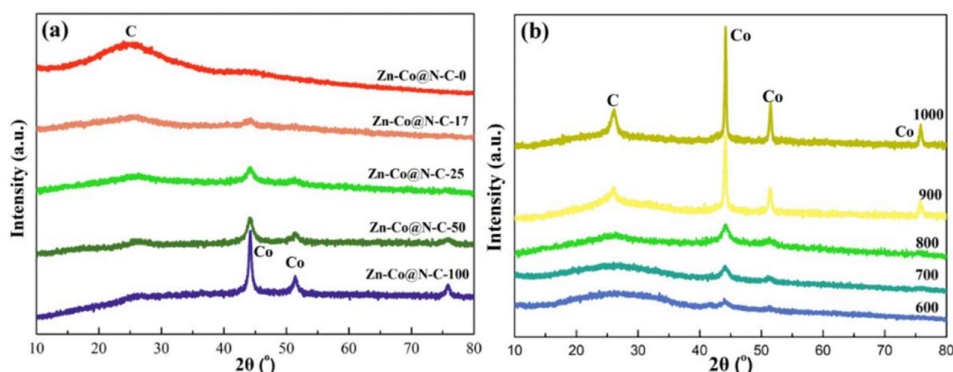


Figure 12: XRD patterns of (a) Zn-Co@N-C-X with different Co contents and (b) Zn-Co@N-C-25-Y with different pyrolysis temperatures. Reproduced from reference [7]

Hengpan Yang and co-workers proposed a method to maximize the utilization of single-atom cobalt sites by constructing a free-standing, cross-linked, and high-yield carbon membrane (CoSA/HCNFs, Cobalt Single Atoms / High yield Carbon Nano Fibres) derived from polymers by a facile and effective electrospinning method. The 3D net-like CoSA/HCNFs nanofibers with continuous porous structure, could facilitate large electrochemical active surface areas and be in favour of the reactant transportation, generating abundant and effective cobalt single atoms for CO₂ reduction. This then was observed to have high utilization of single-atom Co sites eventually leading to CO with 92% Faradaic efficiency and 211 mAcm⁻² [25]. The X-ray absorption near-edge structure (XANES) of CoSA/HCNFs is present between Co foil and Co₃O₄, suggesting the valence state of Co element to be between 0 and +3 (Fig. 2a). Emphasis on one peak at 1.5 Å by extended Fourier-transformed (FT) X-ray absorption fine structure (EXAFS) spectra (Fig. 2c) claimed the existence of a Co–N coordination shell, accompanied by a slight shift of Co₃O₄ to the Co–O peak (1.54 Å). No peak around 2.2 Å of Co–Co were revealed, disclosing that Co atoms did not aggregate to form metal particles. The wavelet transform (WT) curve of CoSA/HCNFs (Fig. 2d-f) shows the WT maximum at 6 Å⁻¹, attributed to the Co–N bond in contrast with Co foil and Co₃O₄. XANES (figure 13) curve showed no maximum intensity peaks for the Co–Co bond observed. Furthermore, cobalt phthalocyanine (CoPc), having a Co-N₄-C structure, revealed a very close valence state and coordination environment to CoSA/HCNFs, another indication of Co-N₄-C in CoSA/HCNFs catalyst [25].

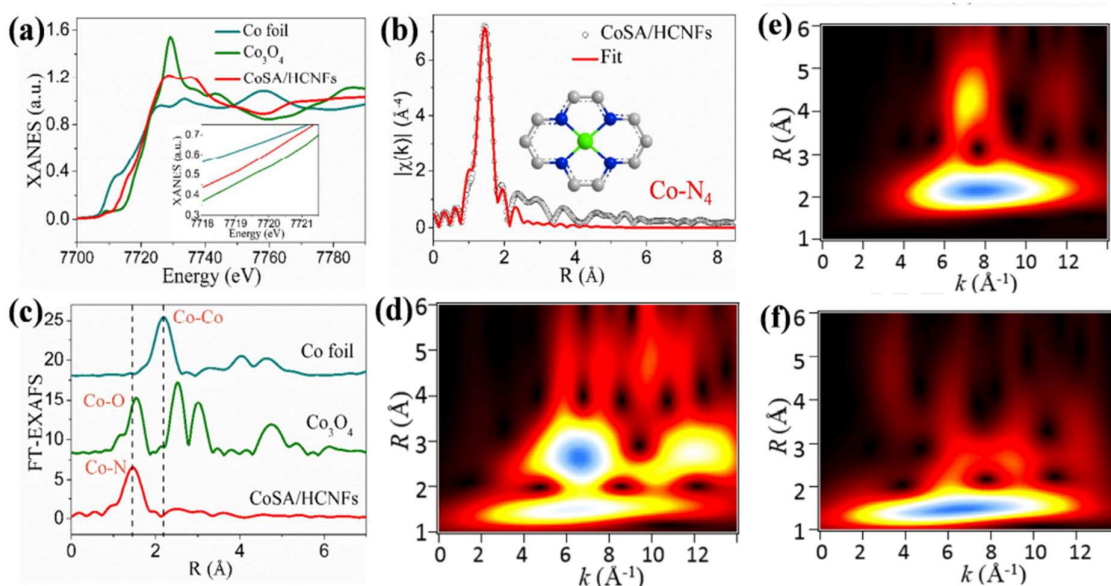


Figure 13: XANES spectra at the Co K-edge (inset is the magnified image) of Co foil, Co₃O₄ and CoSA/HCNFs (a); Fitting for EXAFS data of CoSA/HCNFs, inset is the Co-N₄ structure (b); FT at R space of three samples (c); WT at R space of (d) Co foil, (e) Co₃O₄ and (f) CoSA/HCNFs. Reproduced from reference [25]

Zhang et al. prepared Carbon nanotubes, and cobalt phthalocyanine (CoPc) in DMF (solvent), which was later used for the ER CO_2 giving H_2 and CO as the major products. In this paper sonication of 30 mg of purified CNTs dispersed in 30 ml of DMF was carried out for one hour, followed by adding CoPc or CoPc-CN in DMF into the suspension of CNT. Later, sonicating for 30 min to obtain a heterogenous solution. After stirring the same for 20 h at room temperature, the mixture centrifuged, and precipitate washed with DMF and ethanol and then lyophilized to yield the product [26]. Accordingly, by tuning the CoPc with an electron-withdrawing group like a cyano (CN) group (CoPc-CN/CNT), the electrocatalytic reduction performance of CO_2 increased with faradaic efficiency greater than 95%. Thereafter, hybrid materials of CoPc/CNT and CoPc-CN/CNT had an upper hand as they could provide high geometrical catalytic current densities. Catalytic performance like activity, selectivity, and durability noticed from CoPc/CNT, and CoPc-CN/CNT is due to CNT hybridization on the nanoscale in line with cyano substitution. It was noticed that, due to strong interactions between CoPc-CN (or CoPc) and CNTs, uniform distribution, of molecules on carbon material was discovered [26]. Thus, enabling unmasking of a high degree of catalytic site favourable for achieving high catalytic current densities. During the electrocatalytic process rapid electron transfer from the electrode to surface molecules anchored on CNTs facilitates quick repetitive cycling between Co(II) and Co(I) thereby supporting CO_2 conversion to CO . The cyano substituent (electron-withdrawing group) on the phthalocyanine ligand, facilitates the formation of Co(I) , therefore, considering the active site for reducing CO_2 [26].

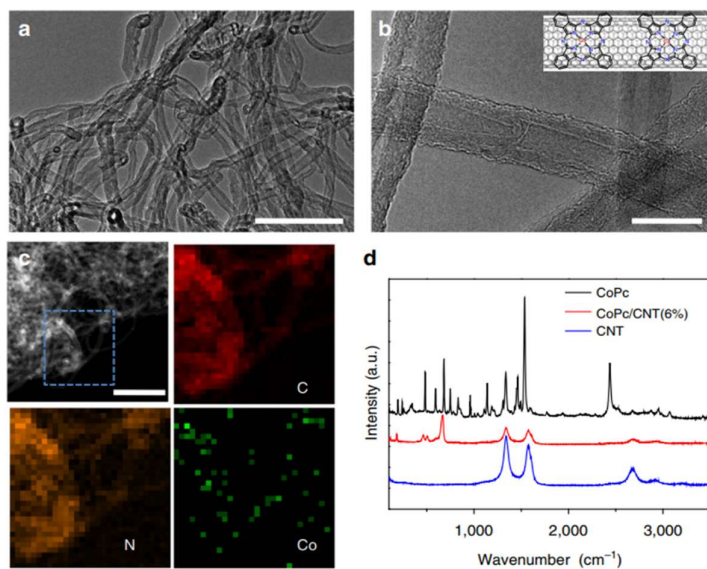


Figure 14: (a,b) TEM images of the CoPc/CNT(6%) hybrid. Inset in b shows a schematic representation of the CoPc/CNT hybrid. (c) STEM image of the CoPc/CNT(6%) material and the corresponding EDS maps of C, N and Co in the blue dash area. (d) Raman spectra of pure CoPc, the CoPc/CNT(6%) hybrid and pure CNTs. Scale bars, 100 nm (a); 20 nm (b); and 200 nm (c). EDS, energy dispersive X-ray spectroscopy; STEM, scanning transmission electron microscopy. Reproduced from reference [26]

To describe hybrid CoPc/CNT, Raman spectroscopy (figure 14 d) was utilized, where some vibrational bands of CoPc were not noticed, suggesting strong CoPc-CNT electronic interactions that prohibit some vibrational modes of the CoPc molecules on CNT [26].

Liwen Wang and co-workers observed that N-doped carbon-loaded transition metal catalysts have unique electrocatalytic performance. Through findings, heterocyclic N-species make close contact with metal, modulating electronic properties of active sites, thereby effectively reducing CO₂. Thus, a ternary hetero-structural catalyst CoO/CN/Ni, with cobalt as catalytic centres, supported on N-doped carbon with underlying nickel was designed, to convert CO₂ to methanol. During synthesis required amount of commercial Vulcan XC-72R was dissipated in acetone, agitated for 3 h at room temperature, filtered, and dried in a vacuum oven at 343 K for 4 hours. Then, in a mixture of 10% nitric acid and 30% hydrogen peroxide ($V_{\text{HNO}_3} : V_{\text{H}_2\text{O}_2} = 2:1$), prepared carbon powder was dispersed and refluxed at 333 K for 5 hours. The carbon support obtained after suction filtering, washing, and drying in a vacuum oven at 353 K [27]. Aqueous solution of nickel nitrate was impregnated to the above carbon using an incipient-wetness impregnation method, then dried at 353 K overnight and calcined at 573 K for 1 h in argon. By encapsulating the polymer of EDTA and CCl₄ on NiO/C and carbonizing in inert atmosphere, composites of Ni NPs capped by CN layer (CN/Ni) were prepared. By ultrasonication, 100 mg NiO/C powder was dispersed in 15 mL m-xylene, after which 250 mg EDTA and 500 mg CCl₄ were added. The suspension stayed at 363 K for 4 h and stabilized 413 K for another 4 h. After cooling, the polymer-coated NiO/C powder was washed with m-xylene and dried at 393 K overnight. The CN/Ni support acquired after carbonizing at 873 K for 6 h and 1173 K for 30 min in flowing N₂. This was then refluxed in 1 M H₂SO₄ at 353 K for 4 h before loading Co NPs to avoid the formation of the nickel oxide compound. 50 mg of CN/Ni powder dispersed in 1mg/mL dopamine solution [prepared by dissolving dopamine hydrochloride in 10 mM tris buffer solution (pH 8.5)]. After stirring, surface-modified CN/Ni support obtained by centrifugation and dehydration. By incipient-wetness impregnation method, deposition of Co NPs on CN/Ni support was done. It was noticed that, nickel underneath the N-doped Carbon (CN) layers, donate electrons to outer CN, creating an electron-enriched modulation on the CoO/CN surface sites, this not only selectively converts CO₂ to methanol but also suppresses hydrogen formation with faraday efficiencies higher than 70% and partial geometrical current density higher than 10 mA/cm² [27].

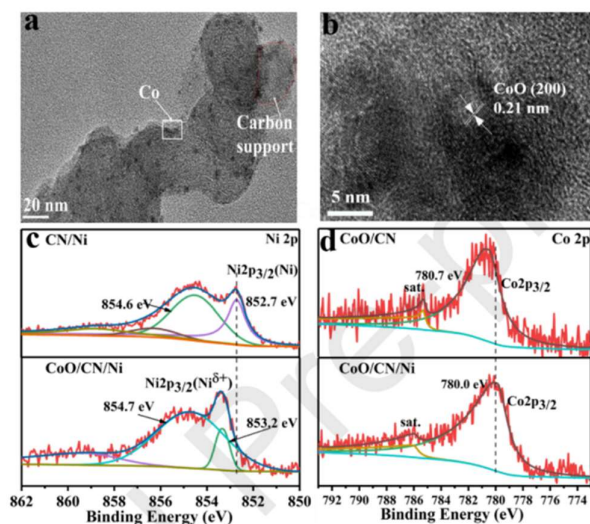


Figure 15: (a) TEM image and (b) HRTEM image of CoO/CN/Ni sample. (c) The XPS spectra: (c) Co 2p region of CoO/CN and CoO/CN/Ni; (d) Ni 2p region of CN/Ni and CoO/CN/Ni. Reproduced from reference [27]

The TEM images (figure 15a) of CN/Ni showcased the distribution of Ni NPs densely and uniformly beneath CN layers. EDX elemental mappings confirm the presence of C, N, O, Ni, and Co in uniformly distributed states [27].

The process of synthesizing syngas consisting of H₂ and CO is of significance in the chemical industry for synfuel production. However, the same requires a large amount of non-renewable energy source. To provide a clean and green method for producing syngas, Huang et al. proposed a simple pyrolysis method by using Co-based N doped carbon to provide an ideal platform to generate syngas with tuneable ratios of H₂ to CO with the highest FE of 56.3% for CO and a total current density of 10.8 mAcm⁻² at -0.9 V vs RHE during CO₂ electrochemical reduction. Structural characterizations proved that the co-existence of CoO and Co²⁺ were responsible for the tuneable syngas synthesis. Here they obtained syngas with the tenable ratios of H₂ to CO ranging from 1:1 to 3:1. LSV curve of Co/N-C-NH₃ FE and current density are seen in figure 16 [28].

Doped heteroatoms in carbons stabilize the key intermediate (*COOH) and lower the Gibbs free energy of *COOH for producing CO during the catalytic process. N-doped carbon materials were widely used, in CO₂ reduction including with other heteroatoms like B, P, S, and F to enhance the property of carbon in promoting CO₂RR. Based on this, Zhenhai Wen and co-workers synthesized, S, N Co-doped carbon nanosheets (termed as NS-CNSs) by a facile salt template approach. In the beginning iron-oleate antecedent was prepared as carbon

precursor, then together with Na₂SO₄ and urea the sample underwent two-step pyrolysis and acid etching steps obtaining nitrogen and sulphur co-doped carbon nanosheets (NS-CNSs)

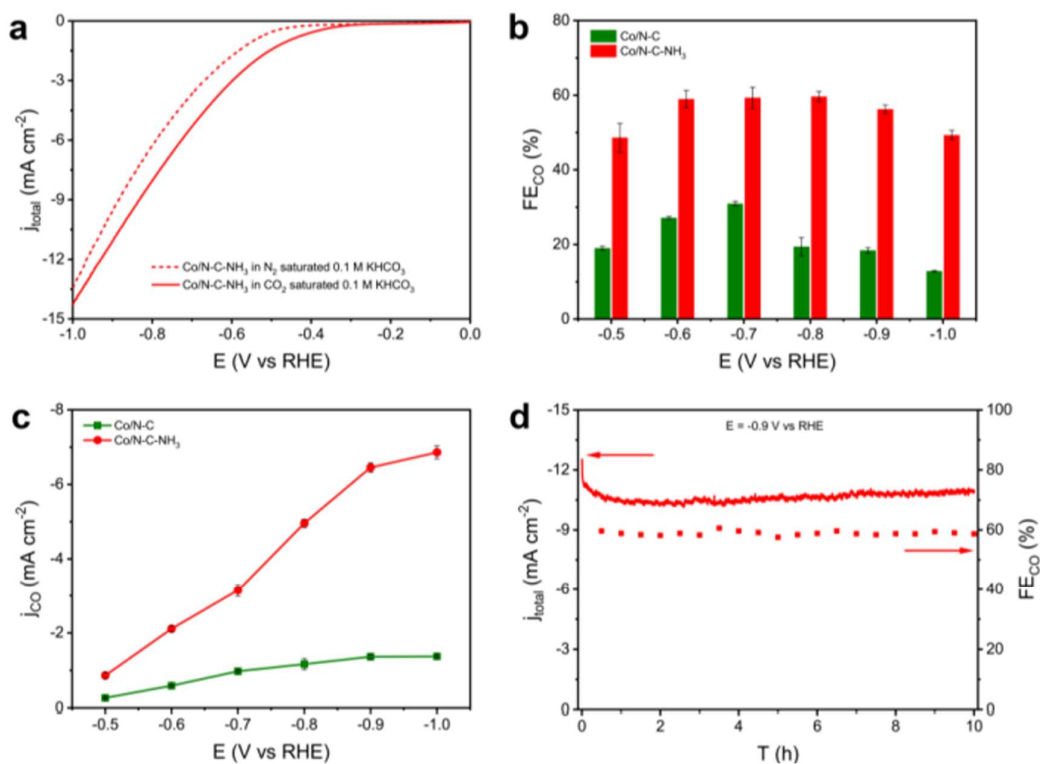


Figure 16: (a) LSV curves of Co/N-C-NH₃ in N₂-saturated and CO₂-saturated 0.1 M KHCO₃. (b) FE and (c) Current density for CO at different potentials on Co/N-C-NH₃ and Co/N-C. (d) 10 h potentiostatic test of Co/N-C-NH₃ at -0.9 V vs RHE. Reproduced from reference [28]

under different temperatures denoted as NS-CNSs-x (x represents the carbonized temperature 800°C, 900°C, 1000 °C, 1100 °C). The prepared dual heteroatoms-doped carbon nanosheets selectively converted CO₂ into CO with a high FE of nearly 85% at -0.55 V vs. RHE. In the formulated 2D structure (mostly found porous) pyridinic N acts as active site for CO₂RR, and the doped S increased the porosity thus, improving catalytic activity [29] SEM and TEM were used to check the morphology of the pyrolyzed product. Acquired NS-CNSs-1000 showcased a folded and layered structure. TEM reaffirmed the 2D nanosheets morphology of the substance [29].

Table 1: Cobalt Catalysts discussed in Literature.

ENTRY	Co CATALYST	REAGENTS	ELECTROLYTE	PRODUCT	POTENTIAL	FE	REF.
1	CoTAPc	MWCNT, ITO electrode, graphite electrode, DMF	KHCO ₃	HCOOH	-0.5 v	78%	[8]
2	Co ₃ O ₄	Co(NO ₃) ₂ , PVA, KOH	KHCO ₃	HCOOH	-2.5 v		[9]
3	Co(II) Cl complex	MWCNT, acetonitrile, Nafion	Na ₂ SO ₄	CO, H ₂	-1.1v	89.00%	[14]
4	Co ₃ O ₄	ZnCl ₂ .2H ₂ O, Co (NO ₃) ₂ , Nafion	KHCO ₃	HCOOH	1.5 v	78.50%	[10]
5	Co ₃ O ₄	NaHCO ₃ , SnCl ₂ .2H ₂ O	KHCO ₃	HCOOH	2.0 v	92.60%	[5]
6	Co ₃ O ₄	[Cu(NO ₃) ₂ .3H ₂ O], [Co(NO ₃) ₂ .6H ₂ O],	KHCO ₃	CH ₃ CH ₂ OH	2.0 v	96.15%	[3]
7	Partially oxidized atomic Co	(CO ₃) _{0.5} (OH).0.11H ₂ O, Co(acac) ₃ , CAB	Na ₂ SO ₄	HCOOH	0.85 v	90.10%	[12]
8	Ultrathin Co ₃ O ₄		KHCO ₃	HCOOH	-0.88 v	60%	[12]
9	Co ₃ O ₄	Crystal violet dye, Nafion	KHCO ₃	HCOOH	2.3 v	45.30%	[11]
10	Co pentadentate complexes	Co and Fe electrode		HCOOH	-1.01 v	82.00%	[16]
11	atomic cobalt layers (V _o -rich)	Co(acac) ₃ , CTAB	Na ₂ SO ₄	HCOOH	-0.87 v	87.60%	[13]
12	CoPc/CNT	MWCNT, DMF	KHCO ₃	CO, H ₂	-0.63 v	over 90%	[24]

Table 1: Cobalt Catalysts discussed in Literature (Continued)

ENTRY	Co CATALYST	REAGENTS	ELECTROLYTE	PRODUCT	POTENTIAL	FE	REF.
13	CoPc/CS-CNT	MWCNT, DMF	KHCO ₃	CO	-0.63 v	over 95%	[24]
14	Co ₃ S ₄ @Co ₃ O ₄ core-shell	Co(NO ₃) ₂ , PPh ₃ , ammonia, Co ₃ S ₄ ,	Na ₂ SO ₄	HCOOH	-0.64 v	85.30%	[17]
15	Co ₃ O ₄ nanofibers	Cl ₂ Co.6H ₂ O, DMF	TBAPF ₆ in ACN	CO	-1.5 v	65.00%	[18]
16	Ag-doped Co ₃ O ₄ (MOF)	AgNO ₃ , Co(NO ₃) ₂ .6H ₂ O	KHCO ₃	CO	-1.8 v	55.60%	[19]
17	In situ exsolved Co nanoparticles	La(NO ₃) ₃ .6H ₂ O, Sr(NO ₃) ₂ , Co(NO ₃) ₂ .6H ₂ O,		CO	1.3 v	95.00%	[21]
18	CoPc	Fe-ZIF-8, CoPc	KOH	CO	0.18 to 0.71 v	Above 90%	[22]
19	Zn-Co@N-C	Co(NO ₃) ₂ .6H ₂ O, Zn(NO ₃) ₂ .6H ₂ O	KHCO ₃	CO	-0.37 to -0.57 v	60%	[7]
20	Single atom CoSA/HCNFs	ZIF-8 nanoparticles, Co(NO ₃) ₂ , PAN	KHCO ₃	CO	-0.9 v	92%	[23]
21	Co ₃ O ₄ @C	SnO ₂ /CC, urea	Na ₂ SO ₄	HCOOH	-1.3v	24.10%	[28]
22	Co-based N doped carbon	Co doped zeolitic imidazolate, NH ₃	KHCO ₃	CO	-0.9 v	56.30%	[26]
23	S, N Co-doped carbon nanosheets	iron oleate, NaSO ₄ , urea	KHCO ₃	CO	-0.55v	85%	[29]
24	CoO/CN/Ni	Cobalt & nickel nitrate	KHCO ₃	CH ₃ OH	-0.3v	70.7%	[27]
25	CoSA/HCNFs nanofibers	ZIF-8 nanoparticles, Co(NO ₃) ₂ , PAN	KHCO ₃		-0.4 -0.9 V	92%	[25]

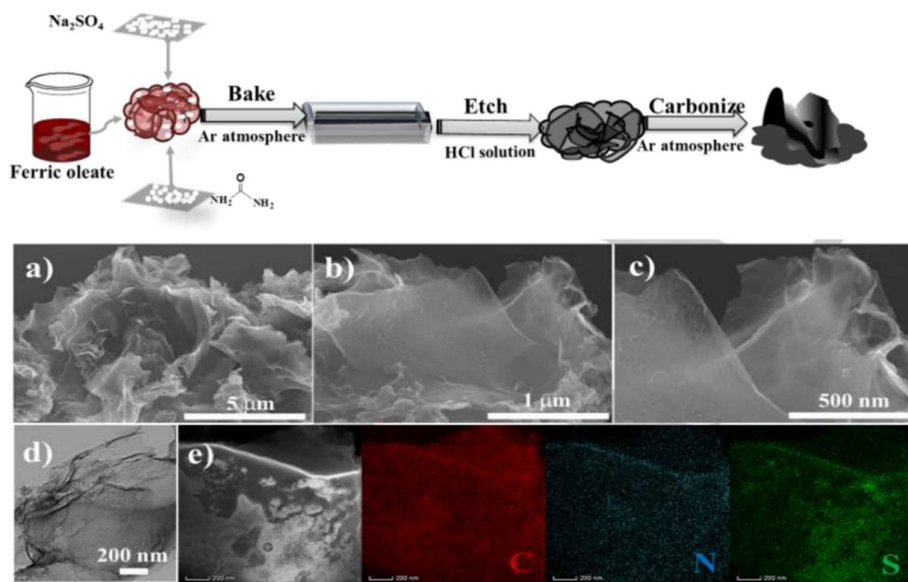


Figure 17: Schematic plot of preparation process of NS-CNSs. (a-c) SEM and (d) TEM images of NS-CNSs-1000, (e) EDS elemental mapping of NS-CNSs-1000. Reproduced from reference [29]

III. CONCLUSION

This mini literature survey summarises the progress in the electrochemical reduction reaction of carbon dioxide using Cobalt-based molecules which include single atom cobalt, partially oxidized cobalt, ultrathin cobalt, Cobalt oxides, cobalt phthalocyanine, and doped Cobalt nanostructures. It was observed that cobalt oxide was not directly used to reduce CO_2 instead, it helped in water oxidation during electrolysis as an anodic electrode whose electrons were used for the reduction of CO_2 . Irrespective of which method used, it is observed that, electrochemical reduction of carbon dioxide requires a large amount of energy for conversion of CO_2 to the product thus, mostly in doing so CO (involving two-electron transfer) is formed as the said requires less energy comparatively than that of the other compounds like methanol, methane, etc.

IV. REFERENCES

- [1] M. Usman *et al.*, "Electrochemical reduction of CO_2 : A review of cobalt based catalysts for carbon dioxide conversion to fuels," *Nanomaterials*, vol. 11, no. 8. MDPI AG, Aug. 01, 2021. doi: 10.3390/nano11082029.
- [2] F. N. Al-Rowaili, A. Jamal, M. S. Ba Shammakh, and A. Rana, "A Review on Recent Advances for Electrochemical Reduction of Carbon Dioxide to Methanol Using Metal-Organic Framework (MOF) and Non-MOF Catalysts: Challenges and Future Prospects," *ACS Sustainable Chemistry and Engineering*, vol. 6, no. 12, pp. 15895–15914, Dec. 2018, doi: 10.1021/acssuschemeng.8b03843.

- [3] V. S. K. Yadav and M. K. Purkait, "Electrochemical Studies for CO₂ Reduction Using Synthesized Co₃O₄ (Anode) and Cu₂O (Cathode) as Electrocatalysts," *Energy and Fuels*, vol. 29, no. 10, pp. 6670–6677, Oct. 2015, doi: 10.1021/acs.energyfuels.5b01656.
- [4] J. P. Collin and J. P. Sauvage, "ELECTROCHEMICAL REDUCTION OF CARBON DIOXIDE MEDIATED BY MOLECULAR CATALYSTS."
- [5] V. S. K. Yadav and M. K. Purkait, "Electrochemical reduction of CO₂ to HCOOH on a synthesized Sn electrocatalyst using a Co₃O₄ anode," *RSC Advances*, vol. 5, no. 84, pp. 68551–68557, Jul. 2015, doi: 10.1039/c5ra12369k.
- [6] S. Gao *et al.*, "Ultrathin Co₃O₄ Layers Realizing Optimized CO₂ Electroreduction to Formate," *Angewandte Chemie*, vol. 128, no. 2, pp. 708–712, Jan. 2016, doi: 10.1002/ange.201509800.
- [7] Z. Miao *et al.*, "Zn-Modified Co@N-C composites with adjusted Co particle size as catalysts for the efficient electroreduction of CO₂," *Catalysis Science and Technology*, vol. 10, no. 4, pp. 967–977, Feb. 2020, doi: 10.1039/c9cy02203a.
- [8] H. Zhao, Y. Zhang, B. Zhao, Y. Chang, and Z. Li, "Electrochemical reduction of carbon dioxide in an MFC-MEC system with a layer-by-layer self-assembly carbon nanotube/cobalt phthalocyanine modified electrode," *Environmental Science and Technology*, vol. 46, no. 9, pp. 5198–5204, May 2012, doi: 10.1021/es300186f.
- [9] S. Singh, C. Mukherjee, and A. Verma, "Development of catalytic activity protocol for electrochemical reduction of carbon dioxide to value added products," *Clean Technologies and Environmental Policy*, vol. 17, no. 2, pp. 533–540, Feb. 2015, doi: 10.1007/s10098-014-0796-6.
- [10] V. S. K. Yadav and M. K. Purkait, "Electrochemical reduction of CO₂ to HCOOH using zinc and cobalt oxide as electrocatalysts," *New Journal of Chemistry*, vol. 39, no. 9, pp. 7348–7354, Jul. 2015, doi: 10.1039/c5nj01182e.
- [11] V. S. K. Yadav and M. K. Purkait, "Simultaneous CO₂ Reduction and Dye (Crystal Violet) Removal Electrochemically on Sn and Zn Electrocatalysts Using Co₃O₄ Anode," *Energy and Fuels*, vol. 30, no. 4, pp. 3340–3346, Apr. 2016, doi: 10.1021/acs.energyfuels.6b00047.
- [12] S. Gao *et al.*, "Partially oxidized atomic cobalt layers for carbon dioxide electroreduction to liquid fuel," *Nature*, vol. 529, no. 7584, pp. 68–71, Jan. 2016, doi: 10.1038/nature16455.
- [13] S. Gao *et al.*, "Atomic layer confined vacancies for atomic-level insights into carbon dioxide electroreduction," *Nature Communications*, vol. 8, Feb. 2017, doi: 10.1038/ncomms14503.
- [14] M. Serhan *et al.*, "Total iron measurement in human serum with a smartphone," in *AICHE Annual Meeting, Conference Proceedings*, 2019, vol. 2019–November. doi: 10.1039/x0xx00000x.
- [15] M. Serhan *et al.*, "Total iron measurement in human serum with a smartphone," in *AICHE Annual Meeting, Conference Proceedings*, 2019, vol. 2019–November. doi: 10.1039/x0xx00000x.
- [16] M. Zhu *et al.*, "Degradation of 4-nitrophenol by electrocatalysis and advanced oxidation processes using Co₃O₄@C anode coupled with simultaneous CO₂ reduction via SnO₂/CC cathode," *Chinese Chemical Letters*, vol. 31, no. 7, pp. 1961–1965, Jul. 2020, doi: 10.1016/j.ccl.2020.01.017.
- [17] N. Iqbal *et al.*, "Cobalt oxide nanoparticles embedded in flexible carbon nanofibers: Attractive material for supercapacitor electrodes and CO₂ adsorption," *RSC Advances*, vol. 6, no. 57, pp. 52171–52179, 2016, doi: 10.1039/c6ra06077c.

- [18] J. Bonin, A. Maurin, and M. Robert, "Molecular catalysis of the electrochemical and photochemical reduction of CO₂ with Fe and Co metal based complexes. Recent advances," *Coordination Chemistry Reviews*, vol. 334. Elsevier B.V., pp. 184–198, Mar. 01, 2017. doi: 10.1016/j.ccr.2016.09.005.
- [19] Y. Yan, K. Li, X. Chen, Y. Yang, and J. M. Lee, "Heterojunction-Assisted Co₃S₄@Co₃O₄ Core–Shell Octahedrons for Supercapacitors and Both Oxygen and Carbon Dioxide Reduction Reactions," *Small*, vol. 13, no. 47, Dec. 2017, doi: 10.1002/smll.201701724.
- [20] "23. Abdalaziz Aljabour (7 feb 2018)".
- [21] S. Y. Zhang, Y. Y. Yang, Y. Q. Zheng, and H. L. Zhu, "Ag-doped Co₃O₄ catalyst derived from heterometallic MOF for syngas production by electrocatalytic reduction of CO₂ in water," *Journal of Solid State Chemistry*, vol. 263, pp. 44–51, Jul. 2018, doi: 10.1016/j.jssc.2018.04.007.
- [22] S. Y. Zhang, J. J. Ma, H. L. Zhu, and Y. Q. Zheng, "Self-supported beaded Au@Co₃O₄nanowire arrays perform electrocatalytic CO₂reduction in water to syngas and water oxidation to O₂," *New Journal of Chemistry*, vol. 44, no. 27, pp. 11808–11816, Jul. 2020, doi: 10.1039/d0nj02179b.
- [23] S. Park *et al.*, "In situ exsolved Co nanoparticles on Ruddlesden-Popper material as highly active catalyst for CO₂ electrolysis to CO," *Applied Catalysis B: Environmental*, vol. 248, pp. 147–156, Jul. 2019, doi: 10.1016/j.apcatb.2019.02.013.
- [24] L. Lin *et al.*, "Synergistic Catalysis over Iron-Nitrogen Sites Anchored with Cobalt Phthalocyanine for Efficient CO₂ Electroreduction," *Advanced Materials*, vol. 31, no. 41, Oct. 2019, doi: 10.1002/adma.201903470.
- [25] H. Yang *et al.*, "Highly efficient utilization of single atoms via constructing 3D and free-standing electrodes for CO₂ reduction with ultrahigh current density," *Nano Energy*, vol. 70, Apr. 2020, doi: 10.1016/j.nanoen.2020.104454.
- [26] X. Zhang *et al.*, "Highly selective and active CO₂ reduction electrocatalysts based on cobalt phthalocyanine/carbon nanotube hybrid structures," *Nature Communications*, vol. 8, Mar. 2017, doi: 10.1038/ncomms14675.
- [27] L. Wang *et al.*, "Ternary heterostructural CoO/CN/Ni catalyst for promoted CO₂ electroreduction to methanol," *Journal of Catalysis*, vol. 393, pp. 83–91, Jan. 2021, doi: 10.1016/j.jcat.2020.11.012.
- [28] M. Huang, X. Kong, C. Wang, Z. Geng, J. Zeng, and J. Bao, "Synthesis of Tunable Syngas on Cobalt-Based Catalysts towards Carbon Dioxide Reduction," *ChemNanoMat*, vol. 7, no. 1, pp. 2–6, Jan. 2021, doi: 10.1002/cnma.202000529.
- [29] G. Wang *et al.*, "Nitrogen and Sulfur Co-doped Carbon Nanosheets for Electrochemical Reduction of CO₂," *ChemCatChem*, vol. 12, no. 8, pp. 2203–2208, Apr. 2020, doi: 10.1002/cctc.201902326.
- [30] C. Chen, J. F. Khosrowabadi Kotyk, and S. W. Sheehan, "Progress toward Commercial Application of Electrochemical Carbon Dioxide Reduction," *Chem*, vol. 4, no. 11. Elsevier Inc, pp. 2571–2586, Nov. 08, 2018. doi: 10.1016/j.chempr.2018.08.019.